A translation of the structure of mussel byssal threads into synthetic materials by the utilization of histidine-rich block copolymers

Enke, Marcel; Bose, Ranjita K.; Zechel, Stefan; Vitz, Jürgen; Deubler, Robert; Garcia, Santiago J.; Van Der Zwaag, Sybrand; Schacher, Felix H.; Hager, Martin D.; Schubert, Ulrich S.

DOI
10.1039/c8py00663f

Publication date
2018

Document Version
Final published version

Published in
Polymer Chemistry

Polymer Chemistry

PAPER

View Article Online
View Journal | View Issue

Cite this: *Polym. Chem.*, 2018, **9**, 3543

A translation of the structure of mussel byssal threads into synthetic materials by the utilization of histidine-rich block copolymers†

Marcel Enke,[a,b] Ranjita K. Bose,‡[c] Stefan Zechel,[a,b] Jürgen Vitz,[a,b] Robert Deubler,[a,b] Santiago J. Garcia,[c] Sybrand van der Zwaag,[c] Felix H. Schacher,[a,b] Martin D. Hager*[a,b] and Ulrich S. Schubert*[a,b]

Received 30th April 2018,
Accepted 31st May 2018

DOI: 10.1039/c8py00663f

rsc.li/polymers

Mussel byssal threads are well-known due to their self-healing ability after the mechanical stress caused by waves. The proposed mechanism demonstrates the importance of reversible histidine–metal interactions as well as the block copolymer-like hierarchical architecture of the underlying protein structure. Taking these two aspects as inspiration for the design of synthetic analogs, different histidine-rich block copolymers were synthesized *via* reversible addition–fragmentation chain transfer (RAFT) polymerization. The hard domain was mimicked using polystyrene and the soft domain consists of *n*-butyl acrylate (BA) as well as histidine moieties as ligands. The block copolymers were crosslinked using different zinc(II) salts and the resulting metallopolymers were investigated with respect to their self-healing abilities. The observed two-step mechanism of the self-healing process was studied in detail. Furthermore, the mechanical properties were determined by nanoindentation and were correlated with other results.

Introduction

Several mussels can produce byssal threads which ensure a steady attachment of the organism to rocks in marine habitats. The extracellular threads are secreted by the mussel foot and can be divided into three parts: the proximal region, the distal region and the adhesive plaque.[1–3] The distal region shows unique mechanical properties and can undergo self-repair after mechanical stress due to reversible histidine–metal interactions ensuring a fast restoration of the mechanical stiffness.[4,5] Block copolymer like proteins, so-called preCols, are well-known building units of mussel byssal threads, in particular of the distal region.[3–6] PreCols consist of clearly defined domains: a central collagen domain, elastic flanking domains and terminal histidine-rich domains. This allows self-assembly into hexagonal bundles and, furthermore, the formation of semi-crystalline domains with the help of crosslinking induced by different metal ions.[7] Interestingly, the threads consist of approximately 95% proteins (dry weight).[8]

A rising number of synthetic approaches have been presented in order to fabricate self-healing polymers inspired by the reversible histidine–metal interactions of the natural byssal threads.[9–15] Recently, the histidine–zinc interactions were investigated in detail with respect to the complexation behavior under different conditions *via* isothermal titration calorimetry (ITC).[14] The results could be clearly associated with the self-healing behavior of histidine-based metallopolymer coatings. Unfortunately, the metallopolymer films were quite soft with weak mechanical properties due to the utilization of poly(lauryl methacrylate) (PLMA) as the backbone.

Mimicking the hierarchical structure of the preCols in synthetic polymers by the utilization of block copolymer structures can result, on the one hand, in an improvement of the self-healing performance and, on the other hand, can lead to improved mechanical properties.[16] Consequently, block copolymers have been utilized with respect to the design of novel self-healing polymers.[12,17–21] For example, Chen *et al.* synthesized a healable soft–hard–soft block copolymer based on hydrogen bonds, in which a reversibly associating unit is introduced into the hard block.[17] Furthermore, Hendrich *et al.* synthesized L-phenylalanine containing block copolymers of methyl acrylate, which revealed healing behavior as well as enhanced mechanical properties.[19] Guan and coworkers fabri-

[a]*Laboratory of Organic and Macromolecular Chemistry (IOMC), Friedrich Schiller University Jena, Humboldtstr. 10, 07743 Jena, Germany. E-mail: martin.hager@uni-jena.de, ulrich.schubert@uni-jena.de*
[b]*Jena Center for Soft Matter (JCSM), Friedrich Schiller University Jena, Philosophenweg 7, 07743 Jena, Germany*
[c]*Novel Aerospace Materials group, Delft University of Technology, Kluyverweg 1, 2629 HS Delft, Netherlands*

†Electronic supplementary information (ESI) available. See DOI: 10.1039/c8py00663f

‡Current address: Engineering and Technology Institute Groningen (ENTEG), University of Groningen, Nijenborgh 4, 9747AG Groningen (Netherlands).

cated multiphase hard–soft brush polymers, which showed improved stiffness and toughness as well as self-healing properties based on hydrogen bonds.[21] Recently, terpyridine containing tri- and pentablock copolymers based on *n*-butyl acrylate (BA) and styrene were presented and the contribution of each block to the overall self-healing behavior was investigated in detail.[22] Interestingly, a two-step mechanism was found for the self-healing process based on the different behaviors of each segment. Nevertheless, a transfer of the mussel byssus design into synthetic polymers (featuring both block copolymer design and reversible histidine–zinc interactions) has to the best of our knowledge not been reported so far. In the current study, we try to go a step further towards a synthetic mussel-inspired analogue by using the block architecture of the mussel and utilized metal–ligand interactions as a blueprint for the design of synthetic healable polymers. Nevertheless, it is a rather simple mimicry compared to the natural archetype; however, it represents a challenging design as well as a further step towards the transfer of natural design principles into synthetic materials.

For this purpose, histidine-rich block copolymers are synthesized in different compositions as well as molar masses using reversible addition–fragmentation chain transfer (RAFT) polymerization with the help of a bifunctional chain transfer agent (CTA), *S*,*S*-dibenzyl trithiocarbonate (DBTTC). The ligand moiety is copolymerized within the soft block (BA). The resulting block copolymers were crosslinked with different zinc(II) salts and quantitative self-healing tests were performed in order to study the kinetics of the self-healing process. In addition, the block copolymers as well as the metallopolymer were investigated using small angle X-ray scattering (SAXS) to account for potential phase separation.

Experimental

Materials and instrumentation

All chemicals used were purchased from Fluka, Aldrich, TCI, Alfa Aesar and ABCR. They were used without further purification. N^{α}-Methacryloyl-N^{τ}-tritylhistidine butyl amide (**1**) was synthesized according to a literature report.[14] *N*-Butyl acrylate and styrene were passed over a short neutral aluminum oxide plug before use. The solvents were dried by refluxing over sodium/benzophenone (toluene) and by treating them with calcium chloride (chloroform and triethylamine). 1D (^{1}H, ^{13}C) nuclear magnetic resonance (NMR) spectra were recorded on a Bruker AC 300 (300 MHz) and a Bruker AC 250 (250 MHz) at 298 K. Chemical shifts are reported in parts per million (ppm, δ scale) relative to the residual signal of the solvent. Coupling constants are given in Hz. Elemental analyses were carried out on a Vario El III (Elementar) elemental analyzer. Size exclusion chromatography (SEC) measurements were performed using a Shimadzu system involving SCL-10A VP (system controller), DGU-14A (degasser), LC-10AD VP (pump), SIL-10AD VP (auto sampler), RID-10A (RI detector), PSS GRAM guard/1000/30 Å (column), DMAc + 0.21% LiCl (eluent), 1 mL min^{-1} at 40 °C (flow rate and temperature), poly(methyl methacrylate) and polystyrene (standard). The TGA analysis was carried out under helium using a STA Netzsch 449 F3 Jupiter and the thermal fluxes during heating were measured on a Netzsch DSC 204 F1 Phoenix under a nitrogen atmosphere with a heating rate of 10 or 20 K min^{-1}. Small angle X-ray scattering (SAXS) measurements were performed on a Bruker AXS Nanostar (Bruker, Karlsruhe, Germany), equipped with a microfocus X-ray source (Incoatec IμS$_{Cu}$ E025, Incoatec, Geesthacht, Germany), operating at λ = 1.54 Å. A pinhole setup with three diaphragms with 750 μm, 400 μm, and 1000 μm holes (with the 1000 μm hole closest to the sample) was used and the sample-to-detector distance was 107 cm. The samples were mounted on a metal rack using Scotch tape. The scattering patterns were corrected for the background (Scotch tape) prior to evaluation. Temperature ramps were performed from 20 to 120 °C in ΔK = 20 steps. The exposure time per isothermal measurement was 2 to 4 h.

The self-healing behavior was studied using a micro-scratch tester (CSM micro-scratch tester). Using a 100 μm diameter Rockwell diamond tip, first a pre-scan at 0.03 N load was performed to gauge the profile of each coating and to subtract the coating inhomogeneity from the scratch depth measurements. Scratches with a total length of 5 mm were produced. A load of 0.5 N and a scratching speed of 2.5 mm min^{-1} resulted in a smooth scratch with a typical width of 200 μm which allowed a clear microscopic analysis of the scratched area during healing. Scratches were made at room temperature. The samples were then observed under an *in situ* microscope and heated at a rate of 50 °C min^{-1} to 100 °C. Micrographs were recorded for the entire duration of the healing process. Image analysis using ImageJ was used to compute the scratch surface area remaining at any time. A constant contrast threshold was chosen for each series of images to ensure consistency in scratch area quantification. Scratch healing was defined as:

$$\%\ \text{Scratch healing} = \left(1 - \frac{A_t}{A_i}\right) \times 100 \qquad (1)$$

where A_t is the surface area of the scratch at a given time and A_i is the initial scratch area.

The samples were sputtered with a thin conductive layer of gold prior to electron microscopy. Scanning electron micrographs (SEM) were recorded using a field emission-scanning electron microscope (FE-SEM) (JEOL, JSM-7500F) equipped with a backscattered electron detector.

The elastic moduli of the materials were characterized *via* depth-sensing indentation (DSI) using a TriboIndenter TI 900 (Hysitron Inc., Minneapolis, MN) with a 2D transducer, equipped with a conospherical diamond indenter tip (~4.7 μm tip radius). Before testing, the polycarbonate standard PC5-218 (Hysitron) was used for calibration and the determination of the area function. The metallopolymer was directly synthesized on a glass cavity slide. Afterwards, the material was dried for one week at ambient temperature and humidity. The depth-sensing indentation (DSI) was conducted under ambient conditions at 23.7 ± 0.8 °C and 22.4 ± 4.3% relative humidity (RH).

For quasi-static testing, a 5 s loading, a 20 s hold at maximum load to eliminate creep effects, and a 5 s unloading profile was applied.[23–25] All the measurements were performed in a single automated run in less than 6 h. The reduced modulus E_r was determined from the unloading response utilizing the analysis method proposed by Oliver and Pharr.[26,27] Measurements were repeated at sixteen maximum loads, increasing in steps of 100 μN from 100 μN to 1600 μN. The values were averaged and measurements outside the area function limits (150 to 2000 nm) were excluded. From the reduced modulus E_r, the indentation modulus E_i was calculated using the elastic modulus and Poisson's ratio of the diamond indenter, 1140 GPa and 0.07, respectively, and a Poisson's ratio of 0.4 for the polymeric material, according to:

$$E_{i,sample} = \frac{1 - \nu_{sample}{}^2}{\frac{1}{E_{r,sample}} - \frac{1 - \nu_{indenter}{}^2}{E_{indenter}}}. \quad (2)$$

The hardness has the normal definition:

$$H = \frac{P_{max}}{A}. \quad (3)$$

Synthesis of the block copolymers

General procedure for the RAFT polymerization (P1 to P8). The desired amounts of the two monomers were dissolved in dry toluene (c = 2 M). Afterwards, exact volumes of the stock solutions of the RAFT agent (CTA; either DBTTC for the preparation of macro-CTAs or the corresponding macro-CTA for the synthesis of the block copolymers) and AIBN were added. The ratio of [CTA] to [AIBN] was always 4/1. The reaction mixture was degassed with nitrogen for 30 min. The reaction was performed at 70 °C for 17 h. All reaction details are summarized in Table S5.† Subsequently, the crude product was purified by preparative size exclusion chromatography (Bio-Beads® S-X1 swollen in chloroform). All analysis details of the polymers are summarized in the ESI.†

General procedure for the synthesis of the metallopolymers (MP1 to MP8). In a 5 mL vial, the desired amount of polymer was dissolved in 1 mL chloroform. A solution of the metal salt in 1 mL methanol was added. The amounts of polymer and the metal salts used are listed in Table 1. The resulting metallopolymers were dried *in vacuo*. The results of elemental analysis and the thermal properties are summarized in Table S1.†

Results and discussion

The goal of this study was the realization of a synthetic look-alike to mimic the structure of mussel byssal threads and the corresponding self-healing behavior in nanostructured coatings. For this purpose, two important properties should be considered. First, the realization of a block copolymer architecture is able to mimic the different domains of the preCols in mussel byssal threads and provide an enhanced mechanical performance. In addition, the introduction of histidine–metal interactions into the material features a temperature-dependent reversibility enabling healing. The histidine–zinc interactions have a relatively low binding strength, presumably resulting in increased self-healing behavior of the supramolecular networks.

For this purpose, N^{α}-methacryloyl-N^{τ}-tritylhistidine butyl amide (**1**) was synthesized according to literature reports (Scheme S1†).[14] Afterwards, the block copolymers were synthesized *via* reversible addition–fragmentation chain transfer polymerization (RAFT). A bifunctional RAFT-agent (*S*,*S*-dibenzyl trithiocarbonate (DBTTC)) was utilized in order to accomplish an A–B–A or B–A–B block structure, where A stands for *n*-butyl acrylate (BA) and B for polystyrene (PS). The utilization of these structures leads to a separate hard block (PS) and a soft block consisting of BA and approximately 10% of the ligand unit (**1**).

In the first step, BA and **1** were copolymerized resulting in **P1** (Scheme 1). Subsequently, styrene was introduced in order to form **P5**. The A–B–A block copolymer features, due to the nature of the RAFT-agent, the hard block as the middle domain and the soft blocks are located at both ends. In addition, a B–A–B block copolymer (**P6**) was synthesized to compare the influence of the block order on the phase separation and self-healing behavior. For this purpose, styrene was first polymerized (**P2**) followed by BA as well as **1** resulting in **P6** (Scheme 1). Furthermore, block copolymers (**P7** (A–B–A) and **P8** (B–A–B)) were synthesized to understand the influence of molar mass and, potentially, to improve the phase segregation as well as the self-healing behavior

Table 1 Overview of the reaction details of the crosslinking reactions (**MP1** to **MP8**)

Metallopolymer	Used polymer	Amount of the polymer [mg]	Used metal salt	Amount of the metal salt [mg]	Ratio His/Zn
MP1	**P5**	52.0	$Zn(OAc)_2$	1.1	3 : 1
MP2	**P5**	51.0	$ZnCl_2$	1.0	2 : 1
MP3	**P6**	53.6	$Zn(OAc)_2$	1.2	3 : 1
MP4	**P6**	51.7	$ZnCl_2$	1.1	2 : 1
MP5	**P7**	55.3	$Zn(OAc)_2$	1.2	3 : 1
MP6	**P7**	59.2	$ZnCl_2$	1.2	2 : 1
MP7	**P8**	55.1	$Zn(OAc)_2$	1.2	3 : 1
MP8	**P8**	58.1	$ZnCl_2$	1.2	2 : 1

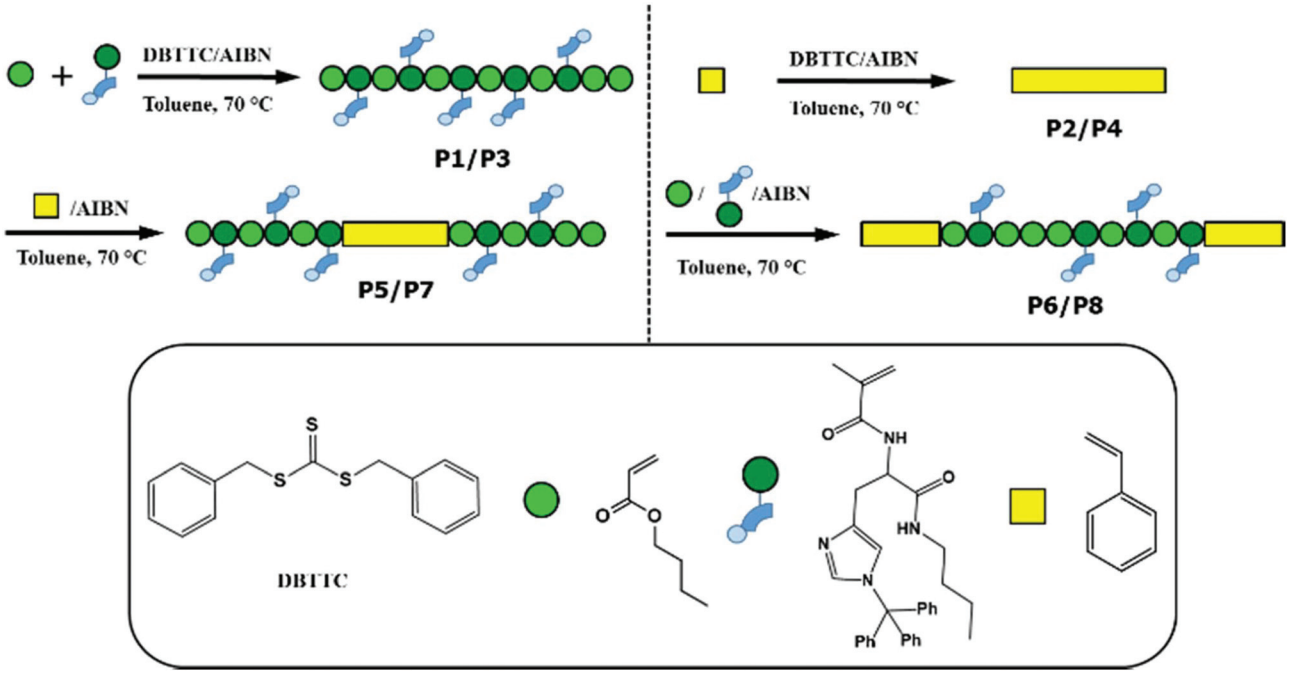

Scheme 1 Schematic representation of the reversible-addition fragmentation chain-transfer polymerization (RAFT) of the block copolymers (block copolymers **P5** and **P7** as well as **P6** and **P8** differ in their molar masses; see also Table 2).

Table 2 Summary of the SEC results (eluent: DMAc + 0.21% LiCl) and the thermal properties of polymers **P1** to **P8** and the resulting ratios of *n*-butyl acrylate (BA) and **1** calculated from ^{1}H NMR

Sample	$M_{n,\,SEC}$ [g mol^{-1}]	$M_{w,\,SEC}$ [g mol^{-1}]	Polymer architecture	$Ratio_{NMR}$ [His] : [BA] : [PS]	$Ratio_{volume}$[c] [hard/soft]
P1	9900[a]	12 400[a]		1 : 10 : 0	—
P2	8900[b]	11 100[b]		0 : 0 : 1	—
P3	24 900[a]	32 400[a]		1 : 10 : 0	—
P4	22 400[b]	28 700[b]		0 : 0 : 1	—
P5	17 200[a]	21 800[a]		1 : 10 : 16	1 : 1.04
	16 800[b]	20 900[b]			
P6	15 100[a]	19 500[a]		1 : 10 : 14	1 : 1.19
	14 900[b]	18 800[b]			
P7	43 800[a]	66 200[a]		1 : 10 : 16	1 : 1.04
	41 500[b]	61 100[b]			
P8	36 100[a]	54 200[a]		1 : 10 : 14	1 : 1.19
	34 600[b]	50 300[b]			

[a] PMMA standard. [b] PS standard. [c] Density of the soft block were determined using a pycnometer (ρ = 1.095 g cm^{-3}; calculation is shown in the ESI).

(Table 2).[28] All block copolymers feature a hard to soft-block ratio of 1 : 1 (ratios were obtained from NMR measurements; for details see the ESI†). The volume ratios of the two block segments (hard : soft) are 1 : 1.04 for **P5** and **P7** and 1 : 1.19 for **P6** and **P8** (Table 2, for calculation see the ESI†). This composition in theory should lead to lamellar structures (calculation of the volume ratio can be found in the ESI†), which are the targeted structures due to their potential improvement of the mechanical properties as well as the healing behavior. For example, poly(isoprene-*block*-styrene-*block*-isoprene) in different compositions revealed the best mechanical properties for lamellar morphologies besides the gyroid morphology, which is not straight-forwardly accessible.[29,30]

Furthermore, the molecular structure within the soft block was further analyzed and for this purpose, the copolymerization of BA and **1** was investigated using a kinetic study by measuring the conversion of both monomers *via* ^{1}H NMR-spectroscopy and size exclusion chromatography (SEC, Fig. S2†).

The distribution of the histidine moieties along the polymer chain is very important to understand the later properties of the block copolymers, *e.g.*, the thermal properties, phase separation or the self-healing behavior of the resulting metallopolymers. The kinetic study revealed that the histidine monomer (**1**) is more rapidly consumed compared with BA, resulting in almost complete conversion of **1** after 4 hours. Afterwards, the reaction kinetics changed significantly leading to a lower increase of the molar mass over time. Such a behavior was also observed for the copolymerization using BA and other ligand monomers.[22] Consequently, the soft block features a gradient distribution of the histidine moieties. Thus, the block copolymers with an A–B–A structure are supposed to show a higher ligand density at the ends of the polymer chains, which is quite similar to the distribution of the histidine units in the mussel byssal threads.[7,31,32] Table 2 summarizes the results of SEC and provides an overview of the respective block copolymer architectures. The thermal properties of all the synthesized polymers are shown in Table S1.† The block copolymers **P5** and **P6** have a molar mass (M_n) of approximately 17 000 g mol^{-1} (Fig. S3 and S4†), whereas this is almost doubled in the case of **P7** and **P8** (Fig. S5 and S6†). Thermal analysis confirmed that all block copolymers are stable up to 300 °C (Fig. S7b– S14b†).[33] In addition, the glass transition temperatures (T_g) of all materials are listed in Table S1† and the DSC curves are depicted in Fig. S7a–S14a.† Furthermore, a detailed description of the thermal behavior of the block copolymers is provided in the ESI.† In addition, small angle X-ray scattering (SAXS) was performed to investigate the A–B–A and B–A–B block copolymers with respect to any potential microphase separation occurring. As already indicated by DSC data, no phase separation was observed in the case of **P5** and **P6**, presumably due to the rather low molar masses. The increased chain lengths of **P7** and **P8** result in a single, broad reflex in SAXS experiments (Fig. S15†), leading to the assumption that the block copolymers do show phase segregation in principle.

Afterwards, the block copolymers **P5** to **P8** were crosslinked with zinc(II) acetate and zinc(II) chloride, respectively. The influence of the ratio of histidine to zinc(II) was previously investigated by isothermal titration calorimetry (ITC)[14] and these values were utilized in the present study. Crosslinking with zinc(II) acetate requires a ligand–metal ratio of 3 : 1 and with zinc(II) chloride a ratio of 2 : 1 (Table 1).[14] All metallopolymers were investigated by elemental analysis (EA), differential scanning calorimetry (DSC) and thermal gravimetric analysis (TGA) and the results are listed in Tables 3 and S2.†

The metallopolymers revealed a thermal stability up to approximately 250 °C (Fig. S16b–S23b†). In general, the glass transition temperatures of the metallopolymers **MP1** to **MP4**, synthesized using the lower molar mass block copolymers (**P5** and **P6**), showed no large variation with respect to the different zinc salts (Fig. S16a–S19a†). This behavior was not observed for the metallopolymers **MP5** to **MP8** (Fig. S20a–S23a†). Here, metallopolymers crosslinked with zinc(II) chloride (**MP6** and **MP8**) revealed a significant higher T_g compared with zinc(II) acetate crosslinked networks (**MP5** and **MP7**). This can be explained by the fact that histidine–zinc interactions have an increased binding affinity when the counter ion is chloride instead of acetate.[14] Thus, the mobility of the polymer chains of the network crosslinked with zinc(II) chloride are more restricted resulting in a higher T_g-value. In addition, the higher molar mass block copolymers exhibit a more distinct phase separation compared to the lower molar mass block copolymers, which presumably intensifies the effect.

The results of all SAXS measurements of the metallopolymers are summarized in Table S3.† The sample preparation was analogous to the self-healing coating preparation in order to ensure comparability. The scattering profiles of **MP1** to **MP6** (Fig. S24,† Fig. 1) revealed no sufficient proof that these metallopolymers are in a phase-separated state. However, the SAXS data of **MP7** and **MP8** (Fig. 1) revealed reflections at 0.28° and 0.62°, roughly corresponding to the [100] and [200] reflections of a corresponding weakly ordered lamellar phase.[34] The phase separation for **MP7** and **MP8** occurs due to the addition of the zinc salt and the corresponding increase of χ. This effect is already known for other block copolymers containing 2-vinylpyridine after the addition of metal salts.[35,36] Moreover, transmission electron microscopy measurements (TEM) as well as atomic force microscopy measurements (AFM) were performed in order to confirm this assumption. Unfortunately,

Table 3 Overview of the thermal properties of metallopolymers **MP1** to **MP8**

Metallo-polymer	Used polymer	Metal salt	Ratio His : Zn	DSC: T_g [°C]	TGA: T_d [°C]	Self-healing efficiency [%] at 100 °C
MP1	**P5**	$Zn(OAc)_2$	3 : 1	51.5	280	51
MP2	**P5**	$ZnCl_2$	2 : 1	51.3	247	58
MP3	**P6**	$Zn(OAc)_2$	3 : 1	36.0	309	97
MP4	**P6**	$ZnCl_2$	2 : 1	31.2	279	84
MP5	**P7**	$Zn(OAc)_2$	3 : 1	76.6	291	99
MP6	**P7**	$ZnCl_2$	2 : 1	105.6	262	61
MP7	**P8**	$Zn(OAc)_2$	3 : 1	78.9	303	65
MP8	**P8**	$ZnCl_2$	2 : 1	91.6	296	71

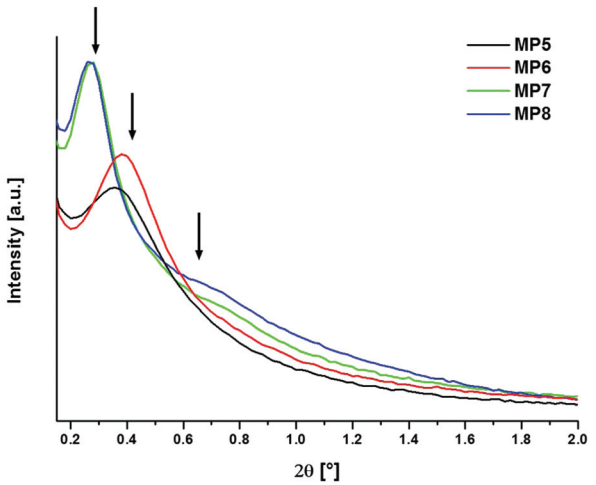

Fig. 1 SAXS data of **MP5** to **MP8**.

the block copolymers are too brittle disabling an accurate sample preparation and, consequently, preventing meaningful TEM/AFM analysis.

Subsequently, the self-healing properties of all metallopolymers were investigated in detail. A micro-scratch tester was utilized to create scratches with well-controlled initial dimensions, which allowed a quantitative calculation of self-healing efficiencies as well as a kinetic study of the self-healing mechanism. These micrographs were analyzed using ImageJ to quantify the remaining scratch surface area at any given time. Due to the utilization of an indirect analysis using image processing, a healing efficiency above 95% is defined as complete healing (slight changes of the color thresholds revealed at this point even more than 100% healing). Fig. S25–S28† depict the obtained self-healing efficiencies for all metallopolymers at 100 °C. In general, all metallopolymers feature a two-step healing mechanism, which was recently described in the literature.[22] The first step of the scratch recovery process is very fast and is mostly completed after five minutes. This step corresponds to the elastic recovery of the polystyrene block.

After this step, 35 to 45% of the scratch is healed, depending on the fraction of polystyrene in the different metallopolymers. The second healing step represents the self-healing process due to the reversibility of the metal–ligand interactions.[22] This two-step healing mechanism was also previously reported for similar block copolymer structures based on polystyrene hard blocks and soft blocks crosslinked with terpyridine complexes.[37]

The metallopolymers differ in the zinc(II) salt used, block copolymer architecture and molar mass. These differences reveal various effects like the phase separation of the different blocks, which influence the self-healing behavior of the metallopolymers. **MP1** to **MP4** contain low molar mass block copolymers, whereas higher molar mass block copolymers are used to prepare **MP5** to **MP8**. The block structures of **MP1** and **MP2** as well as **MP5** and **MP6** are soft–hard–soft (ABA), whereas **MP3** and **MP4** as well as **MP7** and **MP8** have hard–soft–hard (BAB) block copolymer architectures.

For **MP1** and **MP2** a self-healing efficiency of 51% and 58%, respectively (Fig. S25†), could be demonstrated at 100 °C. In contrast, **MP3** achieved complete healing (97%) after 15 minutes and **MP4** featured a plateau at 84% efficiency after 20 minutes (Fig. S26†). The differences in the self-healing abilities can be explained with the various block copolymer architectures. The ABA structure features a central hard block domain and two terminal domains with soft blocks. Thus, the hard block as one unit has an immense influence on the stiffness and on the resulting chain mobility of the polymer chains. In contrast, the BAB block copolymer structure bears the soft block in a central position, whereas the hard block is divided into the two terminal domains (both featuring the half molar mass compared to the ABA structure). Therefore, the ABA block copolymer containing metallopolymers (**MP1** and **MP2**) showed a higher glass transition temperature compared to the BAB block copolymer containing metallopolymers (**MP3** and **MP4**), which lead to a better self-healing at 100 °C for **MP3** and **MP4**.[38]

In contrast, **MP5** to **MP8** represent block copolymers with a doubled molar mass. Here, the ABA block copolymer structure revealed a better self-healing ability. Due to the higher molar masses additional effects like phase separation can influence the self-healing ability. This effect is not present in the metallopolymers **MP1** to **MP4**. For **MP7** and **MP8** a weakly ordered lamellar phase separation was observed, which leads to reduced polymer chain mobility.[16,22] Thus, the self-healing efficiencies at 100 °C are lower compared to those of **MP3** and **MP4**. On the other hand, such a phase separation could not be found for **MP5** and **MP6**. However, the high T_g of **MP6** leads to a lower polymer chain mobility at 100 °C. Nevertheless, **MP5** revealed the lowest T_g compared with metallopolymers based on the higher molar mass block copolymers **P7** and **P8** and, thus, complete self-healing was achieved after 45 min at 100 °C. In summary, at low molar masses the BAB structure is favorable due to the central soft domain, which enables high mobility within the chains. After increasing the molar masses of the polymers, other effects dominate the chain mobility during heating leading to the self-healing mechanism. Here, the BAB block copolymer architecture enables at higher molar mass the introduction of phase separation, which reduces the overall chain mobility and, thus, self-healing results. Therefore, the ABA block copolymer structure at a molar mass of approximately 40 000 g mol^{-1} results in a better self-healing behavior.

MP5 reveals good self-healing behavior as well as a distinct two-step mechanism, which enables a more detailed investigation of the self-healing ability at different temperatures in order to analyze the temperature dependency of the healing mechanism as well as the kinetics of healing (Fig. 2). It was revealed that at 80 °C, very close to the T_g-value of **MP5**, only 74% of the scratch was healed within 360 minutes. Increasing the healing temperature to 100 °C resulted in complete healing (99%) after 45 minutes and a healing temperature of

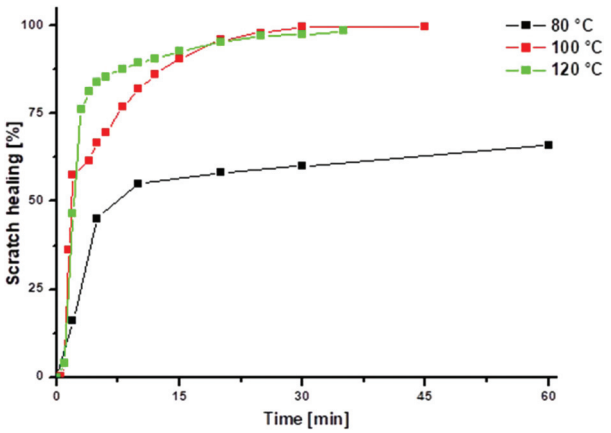

Fig. 2 Quantitative scratch surface recovery of **MP5** at different temperatures between 0 and 60 min (see also Fig. S29† for 0 to 400 min).

120 °C led to a complete healing (99%) after 35 minutes. Consequently, the higher the applied healing temperature, the faster is the healing process. In addition, the healing temperature must be sufficiently greater than the T_g-value of the metallopolymer to achieve complete scratch healing. Furthermore, the two-step self-healing mechanism at 120 °C is indistinct compared with that at 100 °C. In both cases, the viscoelastic contribution of the hard block determined the first step during the first couple of minutes. The second step is caused by the reversible cleavage of the ligand–metal interactions, which is strongly temperature dependent. Thus, the interactions will cleave faster at higher temperatures and, therefore, enable the required mobile phase earlier compared with lower temperatures, which results in a faster self-healing behavior.

Scanning electron microscopy (SEM) was utilized in order to further investigate the two-step healing mechanism of **MP5**. The scratch of **MP5** features a very interesting property compared to all other metallopolymers. Fig. S30† demonstrates the vertical micro-cracks in the scratch area of **MP5**, whereas for example **MP8** revealed a smooth scratch area. It should be noted that the direction of scratching is from right to left in both optical and SEM micrographs. The vertical micro-cracks at the scratch surface heal very fast (Fig. 3) and disappear completely after five minutes (Fig. 4).

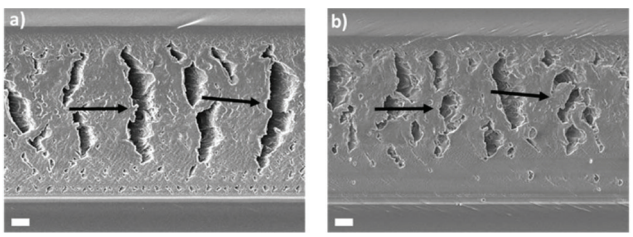

Fig. 3 Optical image of the vertical micro-cracks at the scratch of **MP5**. (a) Scratch before healing and (b) scratch after 20% healing (after 1 min at 100 °C). Scale bars are 10 μm.

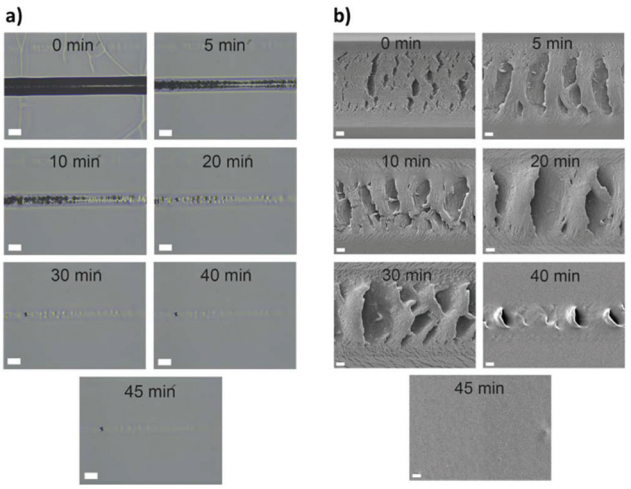

Fig. 4 Optical micrographs (a) and scanning electron micrographs (b) showing two-step scratch healing of **MP5** at different time points upon being heated to 100 °C. Scale bars are 100 μm (a) and 10 μm (b), respectively.

Afterwards, the second step of the self-healing process results in a complete scratch closure. In the second step of scratch healing, the vertical features appear to increase in periodicity from 10 to 30 minutes at 100 °C. This behavior can presumably be attributed to the reorientation of the polymer chains as the crosslinks are reversible. Next, the features reduce in size (40 min) and eventually complete disappearance is achieved.

Thus, the overall healing behavior of the block copolymer is comparable to those of the non-block variants described in the literature.[14] Consequently, the introduction of the hard block domain, *i.e.* polystyrene, does not decrease the ability to close cracks while improving the mechanical properties.

Furthermore, the mechanical properties of the metallopolymer films were investigated by nanoindentation (Fig. S31†), and the properties were found to be comparable to those of the non-block variants described in the literature.[14] Consequently, the introduction of the hard block domain, *i.e.* polystyrene, does not decrease the ability to close cracks while improving the mechanical properties.

The average reduced modulus of the different metallopolymers is between 0.97 and 2.41 GPa and the average hardness is in the range of 0.04 to 0.09 GPa (Table S4†). These values are distinctly higher compared to those of previously presented histidine containing copolymers due to the utilization of the block copolymer structure and, therefore, the introduction of a hard block segment.[14] Furthermore, a comparison with literature examples revealed that this mussel inspired approach resulted in the highest reduced moduli and hardness values showing the high benefit of the combination of the block copolymer structure with metal–ligand interactions.[39,40] In general, networks crosslinked with zinc(II) chloride show an increased value of the reduced modulus compared with zinc(II) acetate containing networks. This behavior is a result of the different ratios between histidine and zinc depending on the

counter ions used.[14] In the case of zinc(II) chloride, a ratio of 2 : 1 (histidine : zinc) is utilized, which results in an increased amount of zinc salt in the metallopolymer, compared with metallopolymers with zinc(II) acetate (ratio: 3 : 1 histidine : zinc). In addition, the utilized block copolymer structure influences the reduced modulus as well as the hardness. Metallopolymers based on a soft–hard–soft block structure demonstrate increased values of both the reduced modulus and the hardness compared with the metallopolymers containing a hard–soft–hard block structure. In the case of the hard–soft–hard block structures, the hard block is divided into two parts, which results in a slight decrease of the mechanical properties. Interestingly, the increase of the molar mass results in a decrease of the mechanical properties. This behavior can be explained with the influence of phase separation on the mechanical properties. It is well-known that the indentation modulus values and the hardness of polymers with different phases, which do not separate, correlate linearly depending on the mass fraction of each individual compound.[41,42] The mechanical values of multiphase copolymers and block copolymers, which show phase separation, do not follow this linear correlation.[14,43–45] Instead, the mechanical values are much lower at the same mass fractions than those expected with the linear correlation. Therefore, **MP5** to **MP8** demonstrate decreased mechanical properties compared to **MP1** to **MP4**.

Conclusions

In this study, block copolymers, aimed to resemble the structure and composition of mussel threads, containing histidine with different molar masses and block sequences were synthesized applying reversible addition–fragmentation chain transfer (RAFT) polymerization. The block copolymers contain polystyrene (PS) as the hard block and poly(*n*-butyl acrylate) (PBA) as the soft segment. The histidine moieties are located within the soft block. The resulting materials were crosslinked with two different zinc salts, zinc(II) acetate and zinc(II) chloride, in order to produce reversible supramolecular networks, which were further investigated with respect to their self-healing properties. The self-healing kinetics were quantitatively studied at 100 °C and a two-step healing mechanism was observed. The self-healing mechanism was related to the viscoelastic response of the hard block upon heating (first step) and the increase of the polymer chain mobility after the reversible cleavage of the metal–ligand interactions. Thereby, **MP3** and **MP5** revealed the best self-healing properties at 100 °C. In addition, scanning electron microscopy (SEM) revealed interesting details of the self-healing behavior of **MP5**. Vertical cracks along the scratch were presented, which heal within short times upon heating. In addition, after the first five minutes, the micro-cracks at the scratch surface disappeared. In addition, SEM images also confirmed the two-step healing mechanism.

In summary, self-healing polymers were investigated and the roles of several factors on the self-healing properties could be elucidated. In this study, the first transfer of the mussel byssal thread structure to synthetic block copolymers is described. The block copolymer architecture is of fundamental importance for the overall healing behavior as well as the mechanical performance, which is much better compared to other self-healing metallopolymers reported to date. Thus, phase separation and polymer chain mobility depend on the block architecture and the molar mass. In the future, different morphologies of the block copolymers could be investigated by varying the block ratios in order to better understand the importance of phase separation during the self-healing process. Furthermore, this first step of mussel inspired polymers shows the high potential of this approach for the design of man-made materials and is, until now, the synthetic structure, which resembles most closely the mussel structure with the corresponding properties, within the limitation of synthetic materials.[46] Thus, it should be expanded, *e.g.*, by introducing other peptides/amino acid sequences into the polymer structure.

Conflicts of interest

There are no conflicts to declare.

Acknowledgements

The authors thank the Deutsche Forschungsgemeinschaft (DFG, SPP 1568) for funding within the framework of the priority program SPP 1568 “Design and Generic Principles of Self-healing Materials”. F. H. S. and U. S. S. are grateful to the Thuringian Ministry for Education, Science, and Culture (TMBWK; #B515-11028, SWAXS-JCSM) for the financial support. S. Z. is grateful to the Carl-Zeiss Foundation for funding.

References

1 E. Vaccaro and J. H. Waite, *Biomacromolecules*, 2001, **2**, 906–911.
2 J. H. Waite, H. C. Lichtenegger, G. D. Stucky and P. Hansma, *Biochemistry*, 2004, **43**, 7653–7662.
3 M. J. Harrington, H. S. Gupta, P. Fratzl and J. H. Waite, *J. Struct. Biol.*, 2009, **167**, 47–54.
4 M. J. Harrington, O. Speck, T. Speck, S. Wagner and R. Weinkamer, *Adv. Polym. Sci.*, 2016, **273**, 307–344.
5 E. Degtyar, M. J. Harrington, Y. Politi and P. Fratzl, *Angew. Chem., Int. Ed.*, 2014, **53**, 12026–12044.
6 T. J. Deming, *Curr. Opin. Chem. Biol.*, 1999, **3**, 100–105.
7 J. H. Waite, X.-X. Qin and K. J. Coyne, *Matrix Biol.*, 1998, **17**, 93–106.
8 M. J. Harrington and J. H. Waite, *Adv. Mater.*, 2009, **21**, 440–444.

9 S. Schmidt, A. Reinecke, F. Wojcik, D. Pussak, L. Hartmann and M. J. Harrington, *Biomacromolecules*, 2014, **15**, 1644–1652.
10 A. Srivastava, N. Holten-Andersen, G. D. Stucky and J. H. Waite, *Biomacromolecules*, 2008, **9**, 2873–2880.
11 D. E. Fullenkamp, L. He, D. G. Barrett, W. R. Burghardt and P. B. Messersmith, *Macromolecules*, 2013, **46**, 1167–1174.
12 D. Mozhdehi, S. Ayala, O. R. Cromwell and Z. Guan, *J. Am. Chem. Soc.*, 2014, **136**, 16128–16131.
13 M. Enke, S. Bode, J. Vitz, F. H. Schacher, M. J. Harrington, M. D. Hager and U. S. Schubert, *Polymer*, 2015, **69**, 274–282.
14 M. Enke, F. Jehle, S. Bode, J. Vitz, M. J. Harrington, M. D. Hager and U. S. Schubert, *Macromol. Chem. Phys.*, 2017, **218**, 1600458.
15 S. C. Grindy and N. Holten-Andersen, *Soft Matter*, 2017, **13**, 4057–4065.
16 S. J. Garcia, *Eur. Polym. J.*, 2014, **53**, 118–125.
17 S. Chen, N. Mahmood, M. Beiner and W. H. Binder, *Angew. Chem., Int. Ed.*, 2015, **54**, 10188–10192.
18 D. Mozhdehi, J. A. Neal, S. C. Grindy, Y. Cordeau, S. Ayala, N. Holten-Andersen and Z. Guan, *Macromolecules*, 2016, **49**, 6310–6321.
19 M. Hendrich, L. Lewerdomski and P. Vana, *J. Polym. Sci., Part A: Polym. Chem.*, 2015, **53**, 2809–2819.
20 M. J. Barthel, T. Rudolph, A. Teichler, R. M. Paulus, J. Vitz, S. Hoeppener, M. D. Hager, F. H. Schacher and U. S. Schubert, *Adv. Funct. Mater.*, 2013, **23**, 4921–4932.
21 Y. Chen, A. M. Kushner, G. A. Williams and Z. Guan, *Nat. Chem.*, 2012, **4**, 467–472.
22 M. Enke, R. K. Bose, S. Bode, J. Vitz, F. H. Schacher, S. J. Garcia, S. van der Zwaag, M. D. Hager and U. S. Schubert, *Macromolecules*, 2016, **49**, 8418–8429.
23 E. F. J. Rettler, J. M. Kranenburg, H. M. L. Lambermont-Thijs, R. Hoogenboom and U. S. Schubert, *Macromol. Chem. Phys.*, 2010, **211**, 2443–2448.
24 M. L. Oyen and R. F. Cook, *J. Mater. Res.*, 2003, **18**, 139–150.
25 M. L. Oyen and R. F. Cook, *J. Mech. Behav. Biomed. Mater.*, 2009, **2**, 396–407.
26 W. C. Oliver and G. M. Pharr, *J. Mater. Res.*, 1992, **7**, 1564–1583.
27 W. C. Oliver and G. M. Pharr, *J. Mater. Res.*, 2004, **19**, 3–20.
28 R. A. Register, *Nature*, 2012, **483**, 167–168.
29 H. Kawai, T. Hashimoto, K. Miyoshi, H. Uno and M. Fujimura, *J. Macromol. Sci., Part B: Phys*, 1980, **17**, 427–472.
30 L. Qiao, C. Leibig, S. F. Hahn and K. I. Winey, *Ind. Eng. Chem. Res.*, 2006, **45**, 5598–5602.
31 M. J. Harrington and J. H. Waite, *J. Exp. Biol.*, 2007, **210**, 4307–4318.
32 S. Krauss, T. H. Metzger, P. Fratzl and M. J. Harrington, *Biomacromolecules*, 2013, **14**, 1520–1528.
33 E. V. Chernikova, A. V. Plutalova, E. S. Garina and D. V. Vishnevetsky, *Polym. Chem.*, 2016, **7**, 3622–3632.
34 B. Chu and B. S. Hsiao, *Chem. Rev.*, 2001, **101**, 1727–1762.
35 Z. Sun, W. Zhang, S. Hong, Z. Chen, X. Liu, S. Xiao, E. B. Coughlin and T. P. Russell, *Polymer*, 2017, **121**, 297–303.
36 J.-Y. Wang, W. Chen and T. P. Russel, *Macromolecules*, 2008, **41**, 4904–4907.
37 R. K. Bose, M. Enke, A. M. Grande, S. Zechel, F. H. Schacher, M. D. Hager, S. J. Garcia, U. S. Schubert and S. van der Zwaag, *Eur. Polym. J.*, 2017, **93**, 417–427.
38 M. D. Hager, P. Greil, C. Leyens, S. van der Zwaag and U. S. Schubert, *Adv. Mater.*, 2010, **22**, 5424–5430.
39 S. Bode, L. Zedler, F. H. Schacher, B. Dietzek, M. Schmitt, J. Popp, M. D. Hager and U. S. Schubert, *Adv. Mater.*, 2013, **25**, 1634–1638.
40 S. Hou and P. X. Ma, *Chem. Mater.*, 2015, **27**, 7627–7635.
41 S. Fakirov, in *Nano- and Micromechanics of Polymer Blends and Composites*, Carl Hanser Verlag GmbH & Co. KG, 2009, pp., 471–516.
42 C. G. Simon, N. Eidelman, Y. Deng and N. R. Washburn, *Macromol. Rapid Commun.*, 2004, **25**, 2003–2007.
43 G. H. Michler, F. J. Baltá-Calleja, I. Puente, M. E. Cagiao, K. Knoll, S. Henning and R. Adhikari, *J. Appl. Polym. Sci.*, 2003, **90**, 1670–1677.
44 A. Flores, F. Ania and F. J. Baltá-Calleja, *Polymer*, 2009, **50**, 729–746.
45 R. Adhikari, G. H. Michler, M. E. Cagiao and F. J. Baltá-Calleja, *J. Polym. Eng.*, 2003, **23**, 177.
46 S. van der Zwaag, N. H. van Dijk, H. M. Jonkers, S. D. Mookhoek and W. G. Sloof, *Philos. Trans. R. Soc., A*, 2009, **367**, 1689–1704.